ACS OMEGA

http://pubs.acs.org/journal/acsodf

Article

Chlorine Atoms of an Aripiprazole Molecule Control the Geometry and Motion of Aripiprazole and Deschloro-aripiprazole in Subdomain IIIA of Human Serum Albumin

Akito Kawai,[#] Yoshihiro Kobashigawa,[#] Kenshiro Hirata, Hiroshi Morioka, Shuhei Imoto, Koji Nishi, Victor Tuan Giam Chuang, Keishi Yamasaki,* and Masaki Otagiri*

Cite This: *ACS Omega* 2022, 7, 29944−29951

Read Online

ACCESS | Metrics & More | Article Recommendations | Supporting Information

ABSTRACT: Aripiprazole (ARP), an antipsychotic drug, binds more strongly to human serum albumin (HSA) than the other ARP derivatives. In addition, the signs for the extrinsic Cotton effects for HSA complexed with ARP or deschloro-ARP are reversed. In this study, we report on a structural−chemical approach using circular dichroism (CD) spectroscopic analysis, X-ray crystallographic analysis, and molecular dynamics simulations. The objective was to examine the relationship between the induced CD spectra and the structural features of the HSA complexes with ARP or deschloro-ARP. The intensity of the induced CD spectra of the HSA complexes with ARP or deschloro-ARP was reduced with increasing temperature. We determined the crystal structure of the HSA complexed with deschloro-ARP in this study and compared it to HSA complexed with ARP that we reported previously. The comparison of these structures revealed that both ARP and deschloro-ARP were bound at the site II pocket in HSA and that the orientation of the molecules was nearly identical. Molecular dynamics simulations indicated that the molecular motions of ARP and deschloro-ARP within the site II pocket were different from one another and the proportion of stacking interaction formations of Tyr411 with the dihydroquinoline rings of ARP and deschloro-ARP was also different. These findings indicate that the induced CD spectra are related to the molecular motions and dynamic interactions of ARP and deschloro-ARP in HSA and may help to understand the molecular recognition and motion that occurs within the binding site for the other HSA ligands more clearly.

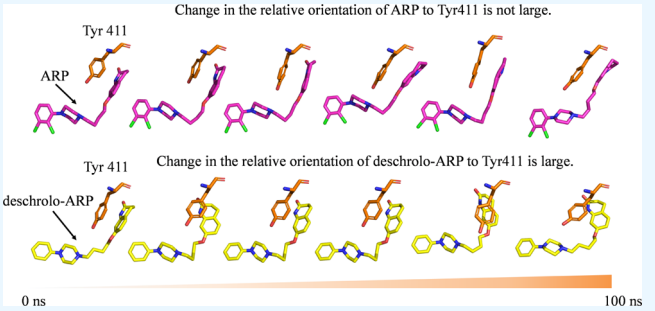

INTRODUCTION

Aripiprazole (ARP), 7-(4-(4-(2,3-dichlorophenyl)-1-piperazinyl)butoxy)-3,4-dihydro-2-(1*H*)-quinolinone, is a novel antipsychotic agent with a different pharmacological profile than other antipsychotics.[1,2] Oshiro et al. reported on the synthesis of a series of 7-(4-(4-substituted phenyl)-1-piperazinyl)butoxy-3,4-dihydro-3(1*H*)-quinolinone derivatives. They also examined the pharmacological activities and toxicities of these compounds.[3,4] Based on the results of a structure−activity relationship study, ARP was found to be a potent and effective agent for treating both the negative and positive symptoms of schizophrenia with fewer clinically adverse effects than the other compounds including risperidone and olanzapine. ARP was marketed in Mexico in 2002 and in Japan in 2006. We recently studied the binding properties of ARP derivatives to plasma proteins as part of a preliminary pharmacokinetic evaluation of these molecules. ARP binds to human serum albumin (HSA) and the α_1-acid glycoprotein.[5−8] ARP binds more strongly to HSA than the other ARP derivatives, and the binding affinity of ARP to HSA (5.94×10^6 M^{-1}) is more than 50 times higher than that of deschloro-ARP (0.10×10^6 M^{-1}).[5] We determined the crystal structure of HSA complexed with ARP, and the results indicated that the binding position of ARP overlaps with the fatty acid binding sites 3 and 4 in HSA.[5] The high binding affinity of ARP to HSA can be attributed to halogen bond interactions between the chlorine atoms at the 3-position of the dichlorophenyl-piperazine group on the ARP molecule and the sulfur atom of Cys392 in HSA.[5]

Interestingly, in the case of the ARP−HSA complex, a positive Cotton effect was observed at about 265 nm and a negative Cotton effect was observed at about 300 nm. In comparison to the ARP−HSA system, small negative peaks at about 268 nm and 295 nm were found for the deschloro-ARP−HSA system. In addition, the heat capacity for the interaction of ARP with HSA was significantly greater than that

Received: May 11, 2022
Accepted: August 9, 2022
Published: August 18, 2022

https://doi.org/10.1021/acsomega.2c02929
ACS Omega 2022, 7, 29944−29951

for the deschloro-ARP−HSA system.[7] These differences in interaction between ARP and deschloro-ARP and HSA led us to hypothesize that the interaction mode of these two ligands with HSA could be different. Thus, in our continuous investigations, we examined the binding geometry of ARP and deschloro-ARP within the binding pocket of HSA using structural−chemical approaches including CD spectroscopic analysis, X-ray crystallographic analysis, and molecular dynamics (MD) simulations.

RESULTS

Temperature Dependency of Extrinsic Cotton Effects for the HSA Interactions with ARP or Deschloro-ARP. We previously reported that the induced CD spectra were observed in the HSA complexes with ARP and its derivatives and that only the deschloro-ARP−HSA complex showed an extrinsic Cotton effect at 265 nm with a reversed sign.[5,6] This reversal in the sign of the extrinsic Cotton effect appears to depend on differences in the structures of ARP and its derivatives, particularly in the presence of chlorine atoms. In this study, we further examined the temperature dependency of the extrinsic Cotton effects generated from the interaction of ARP and deschloro-ARP with HSA. The peak heights and trough depth of the observed CD spectra for both of the HSA complexes with ARP and deschloro-ARP were decreased with increasing temperature (Figure 1 and Table 1), which is indicative of an exothermic reaction. These CD results are consistent with the isothermal titration calorimetry (ITC) results that were previously obtained at this laboratory.[7]

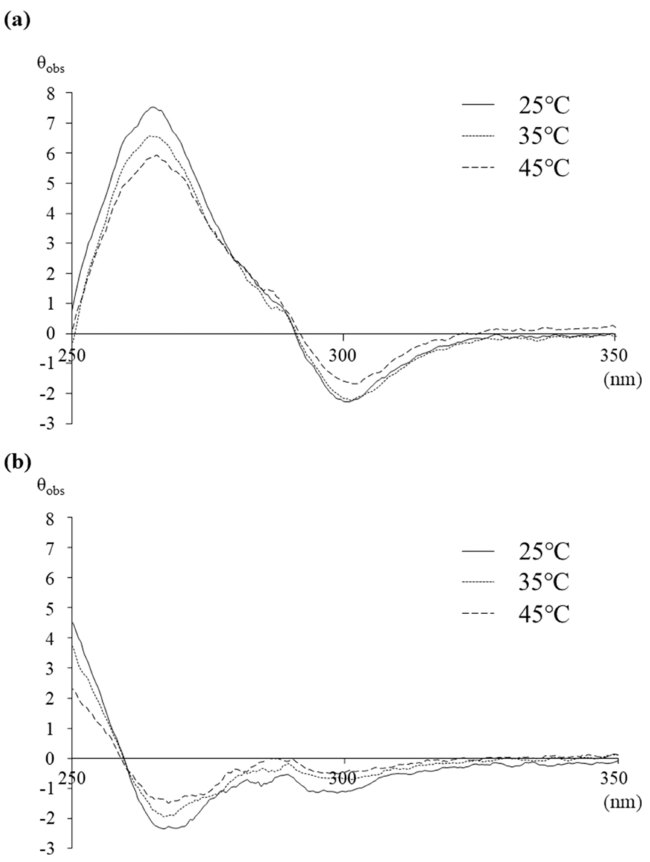

Figure 1. CD spectra of ARP (a) and deschloro-ARP (b) bound to HSA at pH 7.4. The concentration of HSA and each ARP derivative was 30 μM.

Table 1. CD Spectral Characteristics Data for Interaction of ARP and Deschloro-ARP with HSA

	temp (°C)	λ_{max} (nm)	$[\theta_{265,268\ nm}]$ (mdeg·cm^2·mol^{-1})	$[\theta_{300,296\ nm}]$ (mdeg·cm^2·mol^{-1})
ARP	25	265, 300	252 ± 20.1	75.0 ± 6.0
	35		219 ± 17.5	72.9 ± 5.8
	45		191 ± 15.3	53.3 ± 4.3
deschloro-ARP	25	268, 296	75.6 ± 6.1	38.2 ± 3.1
	35		63.6 ± 5.1	21.1 ± 1.7
	45		49.9 ± 4.0	17.5 ± 1.4

Comparison of the Crystal Structures of the HSA Complexes with ARP or Deschloro-ARP. To obtain structural insights regarding the reversal signs of the extrinsic Cotton effects observed in the HSA complexes with ARP and deschloro-ARP, we examined the crystal structures of these complexes. The crystal structure of the HSA−ARP complex was reported previously.[5] The crystal structure of the HSA−deschloro-ARP complex was determined at a 2.10 Å resolution in this study. Data collection and structure refinement statistics are summarized in Table 2.

The crystal structure of the deschloro-ARP−HSA complex revealed that one deschloro-ARP molecule is bound to subdomain IIIA of HSA, the site where the major drug site II ligands are typically bound. A comparison of the structures of the HSA complexes with ARP or deschloro-ARP showed that the binding position of deschloro-ARP coincided with that of ARP in the ARP−HSA binary complex structure and that the binding modes of deschloro-ARP and ARP to HSA are also identical (Figure 2). The dihydroquinoline rings of both ARP and deschloro-ARP share the same binding pocket in subdomain IIIA of HSA, where they participate in stacking interactions with Tyr411. The binding site of phenyl-piperazine groups is located at the opposite binding pocket to the dihydroquinoline binding pocket in subdomain IIIA of HSA. The dihedral angle C2−C1−N1−C10 of the dichlorophenyl-piperazine group of ARP is 108°, and this angle appears to be restricted due to steric hindrance between the piperazine ring and the chlorine atom at the 2-position of the phenyl group. In contrast, the C2−C1−N1−C10 dihedral angle of the phenyl-piperazine group of deschloro-ARP is 15°, suggesting that there is no steric hindrance, presumably because there is no chlorine atom in the phenyl group, thereby allowing the piperazine ring to rotate freely. These results indicate that deschloro-ARP binds to HSA in a manner similar to that for ARP, and the reversal in the signs of the extrinsic Cotton effects is attributed to the difference in the molecular motion of each molecule within the binding pocket. Based on this conclusion, we then analyzed these molecular motions using an MD simulation.

MD Simulation for the Structures of the HSA Complexes with ARP or Deschloro-ARP. MD simulations were initiated from crystal structures of the HSA complexes with ARP or deschloro-ARP. Five runs of 100 ns MD simulations were performed for each complex at 300 K. The results indicated that the mobility of ARP in the binding pocket was restricted and stable, while that for deschloro-ARP was mobile as compared to ARP (Figure 3a,b). To elucidate the nature of the movement of deschloro-ARP in the binding pocket of HSA, we focused on the hydrogen bond between the

https://doi.org/10.1021/acsomega.2c02929
ACS Omega 2022, 7, 29944−29951

Table 2. Data Collection and Structure Refinement Statistics[a]

data set	HSA−deschloro-ARP complex
data collection	
source	SPring-8 BL44XU
wavelength (Å)	0.90000
space group	$P2_1$
unit-cell parameters	
length (Å)	a = 59.3, b = 184.8, c = 59.5
angle (deg)	β = 106.3
resolution range (Å)	50.0−2.10 (2.23−2.10)
no. of observed reflections	492,323 (74,743)
no. of unique reflections	70,209 (11,184)
multiplicity	7.0 (6.7)
completeness (%)	98.7 (97.3)
R_{merge}(%)[b]	5.4 (73.3)
$\langle I/\sigma(I)\rangle$	16.4 (1.92)
refinement	
resolution (Å)	35.9−2.10 (2.13−2.10)
reflection used	70,181 (2705)
R_{work} (%)[c]	21.7 (30.7)
R_{free} (%)[d]	25.5 (34.3)
no. of non-hydrogen atoms	8,714
protein	8,437
ligands	71
solvent	206
r.m.s.d. from ideality	
bond length (Å)	0.004
bond angle (deg)	0.585
average B-factor	68.3
protein	68.5
ligands	69.8
solvent	59.7
Ramachandran plot	
favored region (%)	97.90
allowed region (%)	2.10
outlier region (%)	0.00
clashscore	2.32

[a]Values in parentheses denote the highest resolution shell. [b]$R_{merge} = 100 \times \Sigma_{hkl}\ \Sigma_i|I_i(hkl) - \langle I(hkl)\rangle|/\Sigma_{hkl}\Sigma_i I_i(hkl)$, where $\langle I(hkl)\rangle$ is the mean value of $I(hkl)$. [c]$R_{work} = 100 \times \Sigma_{hkl}||F_o| - |F_c||/\Sigma_{hkl}|F_o|$, where F_o and F_c are the observed and calculated structure factors, respectively. [d]R_{free} is calculated as for R_{work} but for the test set comprising 5% reflections not used in refinement.

N2 atom of the piperazine ring of ARP and the hydroxyl group of the side chain of Tyr411. The results indicated that the proportion of hydrogen bond formation between the N2 atom of the piperazine ring of ARP and the hydroxyl group of the side chain of Tyr411 (a distance of around 2.5 Å and an angle of around 180° in Figure 3c) in the ARP−HSA complex was higher than that for the deschloro-ARP−HSA complex (Figure 3d). The frequency of hydrogen bond formation for the ARP−HSA complex and the deschloro-ARP−HSA complex was determined to be 67.4 and 13.2%, respectively. In addition, the side chain of Tyr411 and the dihydroquinoline ring of ARP formed face-to-face stacking interactions in the ARP−HSA complex (Figure 4a). In the deschloro-ARP−HSA complex, a similar face-to-face stacking interaction between the side chain of Tyr411 and the dihydroquinoline ring of deschloro-ARP was observed, but the angle between the aromatic rings of Tyr411 and the dihydroquinoline ring was widely distributed. Edge-to-face stacking interactions were also observed due to the rotations of the side chain of Tyr411 or the dihydroquinoline ring of deschloro-ARP (Figure 4d). To examine the temperature dependence of the interaction modes between HSA and ARP and deschloro-ARP, we performed the MD simulations for each complex at 363 K. The elevated temperature was assumed to increase the molecular motion of HSA, ARP, and dechloro-ARP and would be expected to allow for the observation of temperature-dependent changes in the dynamic features of the protein complexes within the short MD period (100 ns). The thermal motion of the HSA, ARP, and dechloro-ARP molecules was assumed to be enhanced at 363 K, and HSA was expected to be denatured under physiological conditions at this temperature. However, the time length for the MD simulation was too short to cause the denaturation of the protein. In fact, the time-dependency of the root-mean-square deviation (RMSD) value (Figures S1 and S2), which indicates the structural difference compared to the averaged structure, revealed that the two systems, the ARP−HSA and the deschloro-ARP−HSA complexes, exhibited an obvious fluctuation from 0 to 10 ns, and then, they reached equilibrium and oscillated around the average value. Moreover, the RMSD value was not greatly different between 300 and 363 K, suggesting that the HSA structure remained stable at 363 K. This was assumed to be valid for further analysis. The simulations indicated that, compared to the deschloro-ARP−HSA complex, the face-to-face stacking interactions between Tyr411 and the dihydroquinoline ring of ARP were largely disrupted for both the ARP−HSA and the deschloro-ARP−HSA complexes (Figure 4), while in the ARP−HSA complex, the hydrogen bonding between Tyr411 and the piperazine ring of ARP was largely maintained (Figures 3f,g and S3).

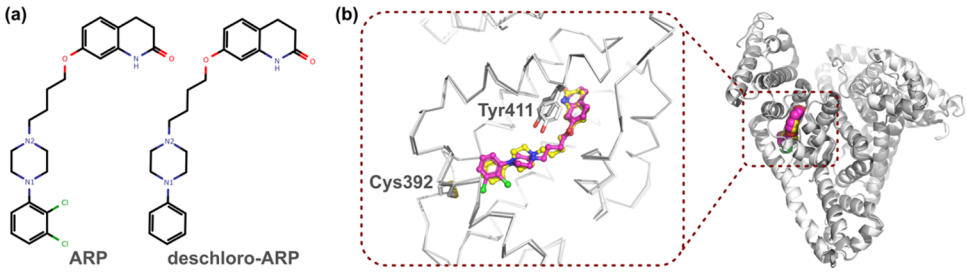

Figure 2. Comparison of the binding of ARP and deschloro-ARP to HSA. (a) Chemical structure of ARP and deschloro-ARP. (b) Structures of the ARP−HSA complex and the deschloro-ARP−HSA complex are colored in gray and white, respectively. The molecules of aripiprazole and deschloro-ARP are shown as ball-and-stick representations and colored in magenta and yellow, respectively.

https://doi.org/10.1021/acsomega.2c02929
ACS Omega 2022, 7, 29944−29951

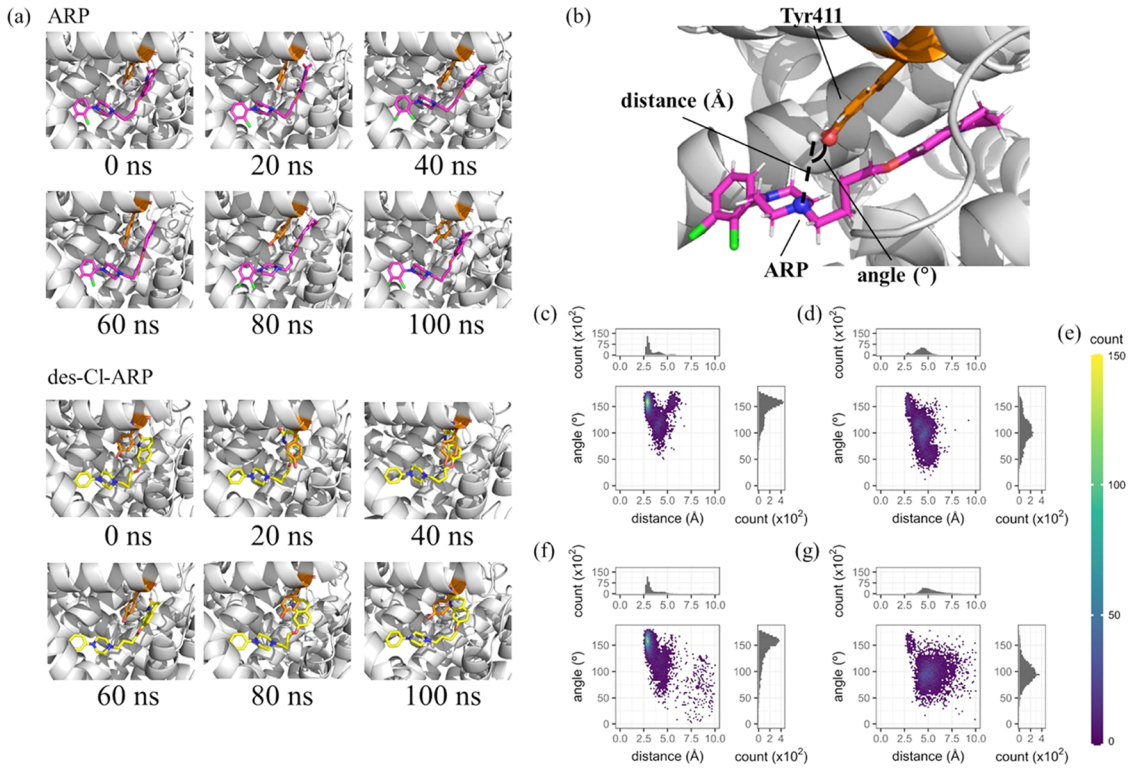

Figure 3. Hydrogen bonding between Tyr411 and the phenyl-piperazine group. (a) Snapshot of the MD calculation around the ARP (upper panel) and deschloro-ARP complexes (lower panel) for every 20 ns at 300 K. (b) "Distance" axis indicates the distance between the oxygen atom of the side chain of Tyr411 and the N2 atom of the piperazine ring, and the "angle" axis indicates the angle between the oxygen atom of the side chain of Tyr411, the hydrogen atom of the side chain of Tyr411, and the N2 atom of the piperazine ring. Each point represents a snapshot from the molecular dynamics simulations colored according to its counts based on the two-dimensional (2D) histograms (c, d, f, g). (c) ARP−HSA complex at 300 K. (d) Deschloro-ARP−HSA complex at 300 K. (e) Scale for the counts on the 2D histogram. (f) ARP−HSA complex at 363 K. (g) Deschloro-ARP−HSA complex at 363 K.

DISCUSSION

We first examined the temperature dependency of the induced CD spectra for the binding of ARP and deschloro-ARP to HSA to elucidate the mode of interaction with HSA for the two ligands. Since ARP is not optically active and HSA does not produce Cotton effects at these wavelengths (250−350 nm), it can be safely assumed that the observed Cotton effects are extrinsic in origin. To clarify the reversal of the signs of the extrinsic Cotton effects, we determined the crystal structure of the deschloro-ARP−HSA complex and compared it to the structure of the ARP−HSA complex structure. The crystal structure of the deschloro-ARP−HSA complex revealed that one deschloro-ARP molecule was bound to subdomain IIIA of HSA, nearly the same site as that for ARP. The binding mode of deschloro-ARP to HSA was also identical to that for ARP (Figure 2). MD simulations initiated from the crystal structures of the HSA complexes with ARP or deschloro-ARP revealed the presence of a stable hydrogen bond between the N2 atom of the piperazine ring of ARP and the hydroxyl group of the side chain of Tyr411 in the ARP−HSA complex. In contrast, this hydrogen bond was disrupted in the case of the deschloro-ARP−HSA complex. This hydrogen bond formation appears to affect the overall molecular motion of ARP or deschloro-ARP within the binding pocket as well as the stacking interactions between Tyr411 and the dihydroquinoline ring of ARP or deschrolo-ARP. These results suggest that the formation and proportion of the stacking interactions between Tyr411 and the dihydroquinoline ring is likely the major cause for the reversal of signs of the extrinsic Cotton effects for the HSA complexes with ARP or deschrolo-ARP. Extrinsic Cotton effects depend on the spatial relationship between the asymmetric center and the perturbed chromophore of the ligand.[9] Schellman reported, based on symmetry rules, that the space around a chromophore could be divided into regions of positive and negative contributions to Cotton effects.[10] The intensities of the observed ellipticities are inversely proportional to the distance between the asymmetrical locus and the perturbed chromophore and the strength of the binding affinity because extrinsic Cotton effects result from electronic interactions. The molecular motion of the ARP or deschloro-ARP molecules in the HSA complex appears to affect the formation and proportion of the stacking interactions between Tyr411 and the dihydroquinoline ring, generating the extrinsic Cotton effect of ARP and its derivatives. Compared to the deschloro-ARP−HSA complex, these observations are consistent with the temperature dependency results in that the stacking interaction between Tyr411 and the dihydroquinoline ring of ARP was found to be largely disrupted in the molecular dynamics simulation at high temperatures for the ARP−HSA complex and the induced CD spectra of the ARP−HSA complexes were decreased with increasing temperature. The ARP molecule bound to HSA was anchored by the halogen bond at the 3-position of the phenyl ring on ARP and the rotation of the piperazine ring was prevented due to the steric hindrance between the chlorine atom at the 2-positon of the phenyl ring on ARP. These restrictions in the molecular motion of deschlro-ARP were not

https://doi.org/10.1021/acsomega.2c02929
ACS Omega 2022, 7, 29944−29951

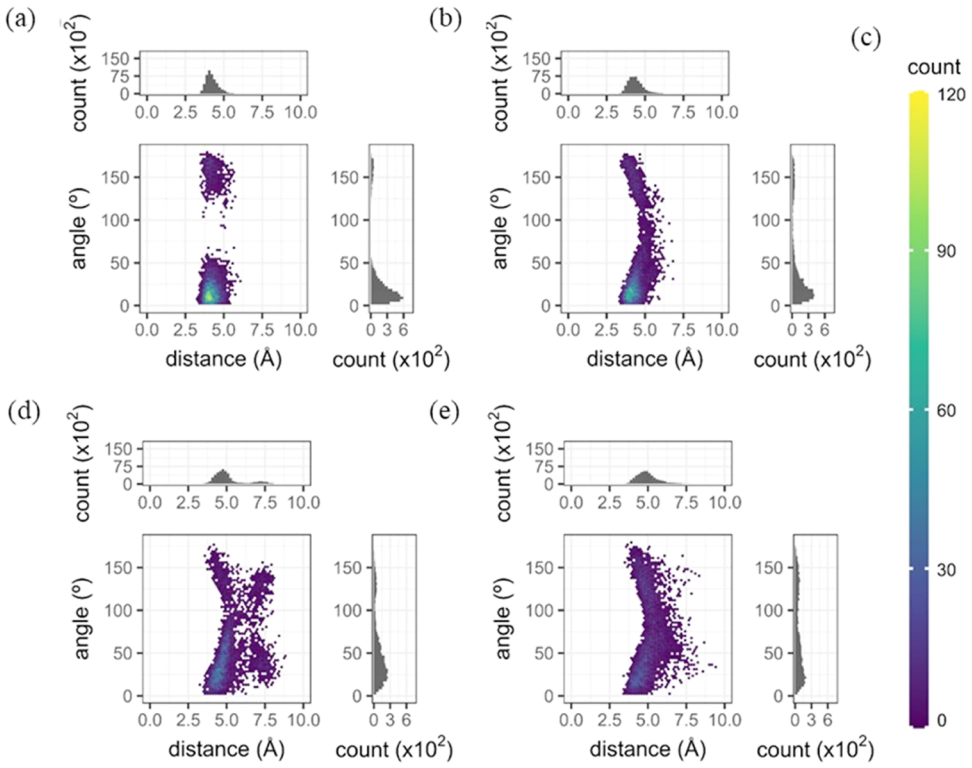

Figure 4. Stacking interactions between Tyr411 and the dihydroquinoline group. The "distance" axis indicates the distance between the centroids of each aromatic ring of Tyr411 and the dihydroquinoline group. The "angle" axis indicates the angle between the normal vectors of each aromatic ring of Tyr411 and the dihydroquinoline group. Each point represents a snapshot from the molecular dynamics simulations colored according to its counts based on the 2D histogram. (a) ARP−HSA complex at 300 K. (b) Deschloro-ARP−HSA complex at 300 K. (c) Scale for the counts on the 2D histogram. (d) ARP−HSA complex at 363 K. (e) Deschloro-ARP−HSA complex at 363 K.

limiting. Consequently, the extrinsic Cotton effects generating different signs could be simplified to depend on the presence of chlorine atoms of ARP. A similar effect by a halogen bond has also been observed in the interaction between HSA and diazepam, a benzodiazepine derivative that also contains a chloro-group.[11] Therefore, the rigidity of the ligand−protein complex plays an important role in the appearance of the induced CD spectra. A loose complex may allow the ligand sufficient freedom of movement, thus weakening the generation of extrinsic Cotton effects. Taking the empirical CD rules and the crystal structure data of the complex into consideration, we conclude that the chlorine atoms control the geometry of the ligand bound to the subdomain pocket of HSA. Drug−albumin binding can be very specific and stereoselective in some cases. This is the reason why HSA is referred to as a silent receptor for drugs and endogenous substances.[12] The limited findings reported herein provide information regarding the role of the HSA molecule in molecular recognition.

CONCLUSIONS

In this study, we investigated the mechanism responsible for the differences in the geometry of ARP and deschloro-ARP within the binding pocket of HSA using CD spectroscopic analysis, X-ray crystal structure analysis, and molecular dynamics simulations. The analysis of the crystal structure and the molecular dynamics simulations indicate that the molecular motions of the ARP molecules and derivatives thereof within the binding pockets differ, and the formation and proportion of the stacking interactions between Tyr411 and the dihydroquinoline ring is the major cause for the reversal signs of the extrinsic Cotton effects for the interaction of HSA with ARP or its derivatives. The chlorine atoms appear to control the geometry and molecular motion of the ligand within the binding pocket of HSA because the strength and the sign of the extrinsic Cotton effects are dependent on the rigidity of the ligand−HSA complex. The limited findings reported in this work will be useful information for understanding the ability of the HSA molecule to recognize different molecules.

EXPERIMENTAL SECTION

Materials. The recombinant HSA was a gift from Nipro Co. (Shiga, Japan). Using a modification of the procedure reported by Chen,[13] HSA was defatted by treatment with activated charcoal at 4 °C in an acidic solution, deionized, and then freeze-dried. Aripiprazole (ARP) was purchased from Tokyo Chemical Industry Co. (Tokyo, Japan). Deschloro-ARP was synthesized following a method reported by Banno et al.[4] All other chemicals were purchased from commercial sources and were of the highest grade available. About 67 mM sodium phosphate buffer (pH 7.4) was used in the equilibrium in the experiments.

Compound Purity. Data on the purity and NMR spectra of the synthesized deschloro-ARP are as reported in previous reports.[5] All other compounds were purchased from commercial sources. Their purities were guaranteed to be more than 95% by each manufacturer.

CD Measurements. CD measurements were carried out using a Jasco model J-1100 spectropolarimeter (Tokyo, Japan),

https://doi.org/10.1021/acsomega.2c02929
ACS Omega 2022, 7, 29944−29951

using a 10 mm cell at 25, 35, and 45 °C. Observed ellipticity (θ) is defined as the ellipticity (in degrees) after subtracting the ellipticity of HSA alone from that of a ligand−HSA within the same wavelength region. The molar ellipticity is defined as the following equation (eq 1), where l is path length and c is ligand concentration.

$$[\Theta] = 100\theta/lc \quad (1)$$

The units for molar ellipticity are millidegrees $cm^2 \cdot dmol^{-1}$. The $[\Theta]$ values were estimated from θ values at 25, 35, 45 °C.

Crystallization of the Deschloro-ARP−HSA Complex. Preparation of the HSA solution for crystallization was performed as described previously.[14] A stock solution of 50 mM deschloro-ARP for the crystallization was prepared by dissolving in DMSO. The deschloro-ARP−HSA complex was formed by mixing the HSA solution and the deschloro-ARP stock solution at a final concentration of 14 μM and 200 μM, respectively, and then, it was incubated at 20 °C overnight. After incubation, excess unbound and insoluble deschloro-ARP deposition was removed by centrifugation (18,000g for 1 h at 4 °C), and the deschloro-ARP−HSA complex was concentrated at 1.4 mM of the HSA concentration using a Vivaspin 500 (MWCO 10,000, Sartorius) centrifugal concentrator. Co-crystallization of the deschloro-ARP−HSA complex was performed using the hanging-drop vapor diffusion method, and deschloro-ARP−HSA crystals for X-ray analysis were obtained by multiple rounds of streak-seeding with droplets prepared by mixing 1.5 μL of the deschloro-ARP−HSAP complex solution and 1.5 μL of the reservoir solution containing 32% (w/v) poly(ethylene glycol) 3350 and 50 mM potassium phosphate pH 7.4 and pre-equilibrated at 4 °C for from one to three days.

Data Collection, Structure Determination, and Refinement. Before the X-ray experiment, the HSA−deschloro-ARP complex crystals were transferred to the cryoprotectant solution containing 34% (w/v) poly(ethylene glycol) 3350 and 50 mM potassium phosphate pH 7.4 and then flash-frozen in liquid nitrogen. Synchrotron experiments were performed at the Photon Factory BL-17A (Tsukuba, Japan) and SPring-8 BL44XU (Harima, Japan). The diffraction data set for the final structure was collected at −173 °C using synchrotron radiation of wavelength 0.9000 Å with an EIGER X 16M detector on SPring-8 BL44XU. The data sets were processed and scaled using XDS.[15] The initial phase of the deschloro-ARP−HSA complex structure was determined by the molecular replacement method using MOLREP[16] from the CCP4 program suite,[17] with the coordinate (PDB: 5YOQ[18]) serving as the search model. Further model building was performed with COOT.[19] Structure refinement, including the refinement of atomic displacement parameters by the translation, liberation, and screw (TLS) method, was performed with phenix.refine.[20] TLS groups were determined using phenix.find_tls_groups from the PHENIX package.[21] The stereochemical quality of the final structure was evaluated by MolProbity.[22] All molecular graphics were prepared using PyMOL (The PyMOL Molecular Graphics System, version 2.0 Schrödinger, LLC.). The atomic coordinates of the deschloro-ARP−HSA complex have been deposited in the Protein Data Bank under the accession code 7X7X.

Molecular Dynamics Simulations. Molecular dynamics simulations of both the ARP−HSA complex and the deschloro-ARP−HSA complex involved the use of Amber 20 and AmberTools 21 software.[23] The ff19SB force field[24] was used for HSA. ARP and deschloro-ARP were generated with GAFF2 and AM1-BCC[25] partial charges using the Antechamber program.[26] The protein−ligand complexes were placed in an octahedron-shaped box with a boundary of 10 Å with a periodic boundary condition filled with TIP3P water. Sodium ions were added to neutralize the system electrically. Equilibration of the system was performed as follows. The generated structure was applied for the energy minimization for only the water with restraining the protein for 2000 cycles, which was followed by heating to 300 or 363 K with the water allowed to move, while the protein was restrained. Next, the entire system was minimized by the steepest descent method and the conjugate gradient algorithm for 2000 cycles, which was heated from 0 to 300 K or 363 K with the NVT ensemble.[27] The system was relaxed at 300 or 363 K for 0.5 ns with the NPT ensemble and the protein heavy atoms restrained. Finally, the system was further relaxed at 300 K for 5 ns with the NPT ensemble.[28,29] Thus, an equilibrated system was used in 100 ns molecular dynamics calculations at 300 or 363 K for both the ARP−HSA and the deschloro-ARP−HSA complexes under periodic boundary conditions. The nonbonded list was generated using an atom-based cutoff of 8 Å. The long-range electrostatic interactions were handled by the particle-mesh Ewald algorithm.[30] The time step of the molecular dynamics simulations was set to 2.0 fs, and the SHAKE algorithm[31] was used to constrain bond lengths of hydrogen.

■ ASSOCIATED CONTENT

Supporting Information

The Supporting Information is available free of charge at https://pubs.acs.org/doi/10.1021/acsomega.2c02929.

Plot of RMSD and snapshot of the MD calculations (PDF)

■ AUTHOR INFORMATION

Corresponding Authors

Keishi Yamasaki − *Faculty of Pharmaceutical Sciences, Sojo University, Kumamoto 860-0082, Japan; DDS Research Institute, Sojo University, Kumamoto 860-0082, Japan;* orcid.org/0000-0003-0537-2367; Email: kcyama@ph.sojo-u.ac.jp

Masaki Otagiri − *Faculty of Pharmaceutical Sciences, Sojo University, Kumamoto 860-0082, Japan; DDS Research Institute, Sojo University, Kumamoto 860-0082, Japan;* Email: otagirim@ph.sojo-u.ac.jp

Authors

Akito Kawai − *Fujita Health University School of Medicine, Toyoake, Aichi 470-1192, Japan*

Yoshihiro Kobashigawa − *Graduate School of Pharmaceutical Sciences, Kumamoto University, Kumamoto 862-0973, Japan*

Kenshiro Hirata − *Faculty of Pharmaceutical Sciences, Sojo University, Kumamoto 860-0082, Japan;* orcid.org/0000-0002-8963-2228

Hiroshi Morioka − *Graduate School of Pharmaceutical Sciences, Kumamoto University, Kumamoto 862-0973, Japan*

Shuhei Imoto − *Faculty of Pharmaceutical Sciences, Sojo University, Kumamoto 860-0082, Japan; DDS Research Institute, Sojo University, Kumamoto 860-0082, Japan*

https://doi.org/10.1021/acsomega.2c02929
ACS Omega 2022, 7, 29944−29951

Koji Nishi − *Faculty of Pharmaceutical Sciences, Sojo University, Kumamoto 860-0082, Japan; DDS Research Institute, Sojo University, Kumamoto 860-0082, Japan*

Victor Tuan Giam Chuang − *Discipline of Pharmacy, Curtin Medical School, Faculty of Health Sciences, Curtin University, Perth, Western Australia 6845, Australia*

Complete contact information is available at: https://pubs.acs.org/10.1021/acsomega.2c02929

Author Contributions

#A.K. and Y.K. contributed equally to this study.

Notes

The authors declare no competing financial interest.

■ ACKNOWLEDGMENTS

Synchrotron experiments were performed with the approval of the Photon Factory Program Advisory Committee (Proposal Nos. 2017G554 and 2019G592) and the Collaborative Research Program of the Institute for Protein Research, Osaka University (Proposal No. 2018B6812). The authors are grateful to the beamline staff for supporting our synchrotron experiments. The computations were carried out using the computer resource offered under the category of General Projects by the Research Institute for Information Technology, Kyushu University.

■ REFERENCES

(1) Burris, K. D.; Molski, T. F.; Xu, C.; Ryan, E.; Tottori, K.; Kikuchi, T.; Yocca, F. D.; Molinoff, P. B. Aripiprazole, a Novel Antipsychotic, Is a High-Affinity Partial Agonist at Human Dopamine D2 Receptors. *J. Pharmacol. Exp. Ther.* **2002**, *302*, 381−389.

(2) Mallikaarjun, S.; Salazar, D. E.; Bramer, S. L. Pharmacokinetics, Tolerability, and Safety of Aripiprazole Following Multiple Oral Dosing in Normal Healthy Volunteers. *J. Clin. Pharmacol.* **2004**, *44*, 179−187.

(3) Oshiro, Y.; Sato, S.; Kurahashi, N.; Tanaka, T.; Kikuchi, T.; Tottori, K.; Uwahodo, Y.; Nishi, T. Novel Antipsychotic Agents with Dopamine Autoreceptor Agonist Properties: Synthesis and Pharmacology of 7-[4-(4-Phenyl-1-Piperazinyl)Butoxy]-3,4-Dihydro-2(1H)-Quinolinone Derivatives. *J. Med. Chem.* **1998**, *41*, 658−667.

(4) Banno, K.; Fujioka, T.; Kucuchi, T.; Oshiro, Y.; Hiyama, T.; Nakagawa, K. Studies on 2(1H)-Quinolinone Derivatives as Neuroleptic Agents I. Synthesis and Biological Activities of (4-Phenyl-1-Piperazinyl)-Propoxy-2(1H)-Quinolinone Derivatives. *Chem. Pharm. Bull.* **1988**, *36*, 4377−4388.

(5) Sakurama, K.; Kawai, A.; Tuan Giam Chuang, V.; Kanamori, Y.; Osa, M.; Taguchi, K.; Seo, H.; Maruyama, T.; Imoto, S.; Yamasaki, K.; Otagiri, M. Analysis of the Binding of Aripiprazole to Human Serum Albumin: The Importance of a Chloro-Group in the Chemical Structure. *ACS Omega* **2018**, *3*, 13790−13797.

(6) Sakurama, K.; Nishi, K.; Imoto, S.; Hashimoto, M.; Komatsu, T.; Morita, Y.; Taguchi, K.; Otagiri, M.; Yamasaki, K. Further Evidence Regarding the Important Role of Chlorine Atoms of Aripiprazole on Binding to the Site II Area of Human Albumin. *J. Pharm. Sci.* **2019**, *108*, 1890−1895.

(7) Nishi, K.; Sakurama, K.; Kobashigawa, Y.; Morioka, H.; Udo, N.; Hashimoto, M.; Imoto, S.; Yamasaki, K.; Otagiri, M. Interaction of Aripiprazole With Human A1-Acid Glycoprotein. *J. Pharm. Sci.* **2019**, *108*, 3911−3916.

(8) Hirata, K.; Ikeda, T.; Watanabe, H.; Maruyama, T.; Tanaka, M.; Chuang, V. T. G.; Uchida, Y.; Sakurama, K.; Nishi, K.; Yamasaki, K.; Otagiri, M. The Binding of Aripiprazole to Plasma Proteins in Chronic Renal Failure Patients. *Toxins* **2021**, *13*, No. 811.

(9) Chignell, C. F. Optical Studies of Drug-Protein Complexes. 3. Interaction of Flufenamic Acid and Other N-Arylanthranilates with Serum Albumin. *Mol. Pharmacol.* **1969**, *5*, 455−462.

(10) Schellman, J. A. Symmetry Rules for Optical Rotation. *Acc. Chem. Res.* **1968**, *1*, 144−151.

(11) Ghuman, J.; Zunszain, P. A.; Petitpas, I.; Bhattacharya, A. A.; Otagiri, M.; Curry, S. Structural Basis of the Drug-Binding Specificity of Human Serum Albumin. *J. Mol. Biol.* **2005**, *353*, 38−52.

(12) Muller, W. E.; Wollert, U. Human Serum Albumin as a "Silent Receptor" for Drugs and Endogenous Substances. *Pharmacology* **1979**, *19*, 59−67.

(13) Chen, R. F. Removal of Fatty Acids from Serum Albumin by Charcoal Treatment. *J. Biol. Chem.* **1967**, *242*, 173−181.

(14) Kawai, A.; Chuang, V. T. G.; Kouno, Y.; Yamasaki, K.; Miyamoto, S.; Anraku, M.; Otagiri, M. Crystallographic Analysis of the Ternary Complex of Octanoate and N-Acetyl-l-Methionine with Human Serum Albumin Reveals the Mode of Their Stabilizing Interactions. *Biochim. Biophys. Acta, Proteins Proteomics* **2017**, *1865*, 979−984.

(15) Kabsch, W. XDS. *Acta Crystallogr., Sect. D: Biol. Crystallogr.* **2010**, *66*, 125−132.

(16) Vagin, A.; Teplyakov, A. Molecular Replacement with MOLREP. *Acta Crystallogr., Sect. D: Biol. Crystallogr.* **2010**, *66*, 22−25.

(17) Winn, M. D.; Ballard, C. C.; Cowtan, K. D.; Dodson, E. J.; Emsley, P.; Evans, P. R.; Keegan, R. M.; Krissinel, E. B.; Leslie, A. G. W.; McCoy, A.; McNicholas, S. J.; Murshudov, G. N.; Pannu, N. S.; Potterton, E. A.; Powell, H. R.; Read, R. J.; Vagin, A.; Wilson, K. S. Overview of the CCP4 Suite and Current Developments. *Acta Crystallogr., Sect. D: Biol. Crystallogr.* **2011**, *67*, 235−242.

(18) Kawai, A.; Yamasaki, K.; Enokida, T.; Miyamoto, S.; Otagiri, M. Crystal Structure Analysis of Human Serum Albumin Complexed with Sodium 4-Phenylbutyrate. *Biochem. Biophys. Rep.* **2018**, *13*, 78−82.

(19) Emsley, P.; Lohkamp, B.; Scott, W. G.; Cowtan, K. Features and Development of Coot. *Acta Crystallogr., Sect. D: Biol. Crystallogr.* **2010**, *66*, 486−501.

(20) Afonine, P. V.; Grosse-Kunstleve, R. W.; Echols, N.; Headd, J. J.; Moriarty, N. W.; Mustyakimov, M.; Terwilliger, T. C.; Urzhumtsev, A.; Zwart, P. H.; Adams, P. D. Towards Automated Crystallographic Structure Refinement with Phenix.Refine. *Acta Crystallogr., Sect. D: Biol. Crystallogr.* **2012**, *68*, 352−367.

(21) Liebschner, D.; Afonine, P. V.; Baker, M. L.; Bunkoczi, G.; Chen, V. B.; Croll, T. I.; Hintze, B.; Hung, L. W.; Jain, S.; McCoy, A. J.; Moriarty, N. W.; Oeffner, R. D.; Poon, B. K.; Prisant, M. G.; Read, R. J.; Richardson, J. S.; Richardson, D. C.; Sammito, M. D.; Sobolev, O. V.; Stockwell, D. H.; Terwilliger, T. C.; Urzhumtsev, A. G.; Videau, L. L.; Williams, C. J.; Adams, P. D. Macromolecular Structure Determination Using X-Rays, Neutrons and Electrons: Recent Developments in Phenix. *Acta Crystallogr., Sect. D: Struct. Biol.* **2019**, *75*, 861−877.

(22) Williams, C. J.; Headd, J. J.; Moriarty, N. W.; Prisant, M. G.; Videau, L. L.; Deis, L. N.; Verma, V.; Keedy, D. A.; Hintze, B. J.; Chen, V. B.; Jain, S.; Lewis, S. M.; Arendall, W. B.; Snoeyink, J.; Adams, P. D.; Lovell, S. C.; Richardson, J. S.; Richardson, D. C. MolProbity: More and Better Reference Data for Improved All-Atom Structure Validation. *Protein Sci.* **2018**, *27*, 293−315.

(23) Case, D.; Aktulga, H. M.; Belfon, K.; Ben-Shalom, I.; Brozell, S.; Cerutti, D.; Cheatham, T.; Cruzeiro, V.; Darden, T.; Duke, R.; Giambasu, G.; Gilson, M.; Gohlke, H.; Götz, A.; Harris, R.; Izadi, S.; Izmailov, S.; Jin, C.; Kasavajhala, K.; Kollman, P. *Amber 2021*, 2021.

(24) Tian, C.; Kasavajhala, K.; Belfon, K. A. A.; Raguette, L.; Huang, H.; Migues, A. N.; Bickel, J.; Wang, Y.; Pincay, J.; Wu, Q.; Simmerling, C. Ff19SB: Amino-Acid-Specific Protein Backbone Parameters Trained against Quantum Mechanics Energy Surfaces in Solution. *J. Chem. Theory Comput.* **2020**, *16*, 528−552.

(25) Jakalian, A.; Jack, D. B.; Bayly, C. I. Fast, Efficient Generation of High-Quality Atomic Charges. AM1-BCC Model: II. Parameterization and Validation. *J. Comput. Chem.* **2002**, *23*, 1623−1641.

(26) Wang, J.; Wang, W.; Kollman, P. A.; Case, D. A. Automatic Atom Type and Bond Type Perception in Molecular Mechanical Calculations. *J. Mol. Graph. Model.* **2006**, *25*, 247−260.

(27) Berendsen, H. J. C.; Postma, J. P. M.; Van Gunsteren, W. F.; Dinola, A.; Haak, J. R. Molecular Dynamics with Coupling to an External Bath. *J. Chem. Phys.* **1984**, *81*, 3684.
(28) Pastor, R. W.; Brooks, B. R.; Szabo, A. An Analysis of the Accuracy of Langevin and Molecular Dynamics Algorithms. *Mol. Phys.* **1988**, *65*, 1409−1419.
(29) Izaguirre, J. A.; Catarello, D. P.; Wozniak, J. M.; Skeel, R. D. Langevin Stabilization of Molecular Dynamics. *J. Chem. Phys.* **2001**, *114*, 2090.
(30) Salomon-Ferrer, R.; Götz, A. W.; Poole, D.; Le Grand, S.; Walker, R. C. Routine Microsecond Molecular Dynamics Simulations with AMBER on GPUs. 2. Explicit Solvent Particle Mesh Ewald. *J. Chem. Theory Comput.* **2013**, *9*, 3878−3888.
(31) Ryckaert, J. P.; Ciccotti, G.; Berendsen, H. J. C. Numerical Integration of the Cartesian Equations of Motion of a System with Constraints: Molecular Dynamics of n-Alkanes. *J. Comput. Phys.* **1977**, *23*, 327−341.

https://doi.org/10.1021/acsomega.2c02929
ACS Omega 2022, 7, 29944−29951